Korean J. Chem. Eng., **27**(2), 390-398 (2010)
DOI: 10.1007/s11814-010-0083-0

Hydrodynamic behavior of an electrified thin film flowing down an inclined plane at high Reynolds numbers

Sunyoung Park and Hyo Kim†

Department of Chemical Engineering, University of Seoul, 90 Jeonnong-dong, Dongdaemun-gu, Seoul 130-743, Korea
(*Received 29 May 2009 • accepted 1 September 2009*)

Abstract−To answer the questions on the dynamics of thin liquid flow down an inclined plane at high Reynolds numbers subjected to a uniform normal electrostatic field, we have derived evolution equations describing the free-surface behavior by using the von Kármán-Pohlhausen approximation. The integration of the evolution equations is numerically performed to address two-dimensional finite-amplitude surface-wave propagation modes. The growth of a periodic disturbance is first examined to compare with the results linear-stability theory, and then to investigate the nonlinear surface-wave behavior the evolution equations are solved numerically by a Fourier-spectral method. For small evolution time the computed nonlinear modes of instability are well consistent with the results from the linear theory. The effect of an electrostatic field makes the flow system significantly unstable.

Key words: Hydrodynamic Behavior, High Reynolds Number, Electrostatic Field, von Kármán-Pohlhausen Approximation, Fourier-spectral Method

INTRODUCTION

Recently, the behavior of an electrified thin liquid film has attracted much attention in engineering application fields such as the cooling of thin liquid film radiators, microelectronics structure formation and pattern transfer, and bio-separation systems due to the combined effects of its high transfer rate and electrically induced instability. Running liquid film always becomes unstable as the flow rates increase whether the system is electrified or not. Without any electric effects the study of the thin liquid layers flowing under a gravitational force down an inclined isothermal plane was initiated by Benjamin [1] and Yih [2]. They identified regimes of linear stability as a function of the Reynolds number and the superimposed wavenumber. After that time quite a number of studies for the thin film flows have been made by a lot of researchers extended to the nonlinear flow regimes.

For an advanced and improved application of the thin film flow, an electrostatic field has been coupled with the dynamics of fluid flowing system. Kim et al. [3] first examined the interaction of an electrostatic field on a flowing liquid-metal film on a plane of an inclined surface. The electrostatic field exerts a tensile force on the liquid film, pulling it away from a puncture that probably occurred on the radiator shell due to micrometeorite impacts in space. Kim [4] also performed a long-wave analysis of the film flow under an electrostatic field to explain the questions about the nonlinear instabilities in a small Reynolds-number flow. In addition, focusing on the view points of nonlinear dynamics Kim [5] explored the behavior of pulse-like solitary waves and Kim et al. [6] examined hydraulic-jump phenomena by using global bifurcation theories on the electrified thin-film plane flow. It was found that the charged electrostatic field always made the flow system more unstable in proportion to the applied amount of electric strength. The solutions of the film height equation proposed by Kim et al. [3] were compared with the experimental measurements of thin film of oil flowing down a nearly vertical plate subjected to a strong normal electrostatic field by Griffing et al. [7] in 2006. Their two-dimensional height profiles measured by fluorescence imaging were very similar to the calculations by Kim et al. [3]. Other applications of electric field can be found recently in the polymer film processing to get a desirable structure formation and pattern transfer. Schäffer et al. [8] showed a simple electrostatic technique to create and replicate lateral structures in polymer films on a submicrometer length scale. In addition to this, in 2001 Schäffer et al. [9] exploited the wave pattern caused by an electrohydrodynamic instability to get a non-equilibrium pattern formation in quasi-two-dimensional systems. Lin et al. [10] reported a systematic characterization of structure formation at the interface of liquid/liquid bilayers in an electric field. These researches have used the surface deformation effect made by the electrohydrodynamic instability. As a new application research topic, Blyth [11] solved the linear stability problem describing the effect of an electric field on a contaminated film flow down an inclined plane. He showed the major competition between the stabilizing influence of an insoluble surfactant and the destabilizing influence of an electric field on the film flow by applying two-dimensional disturbance theory.

The previous researches are mainly focused on the small Reynolds-number flow system, that is, the order of Reynolds number is assumed unity and the flow system is analyzed by the lubrication theory. As Reynolds number becomes larger up to one order of magnitude in ξ, i.e., $O(1/\xi)$ (For the applications under any engineering considerations a larger Reynolds may be necessary) where the flow is still laminar and the small parameter ξ ($<<1$) is defined later, we cannot solve systematically the governing equations of

†To whom correspondence should be addressed.
E-mail: hkim@uos.ac.kr

the fluid because the inertial force terms are balanced with the viscous shear force term. Hence in order to obtain an analytic evolution equation we need to use the von Kármán-Pohlhausen approximation successfully employed by Rahman et al. [12] and Prokopiou et al. [13], etc.

The aim of the present work is to address the questions concerning the hydrodynamics of the electrified thin film flow down an inclined plane under gravity in the limit of large Reynolds number. From the acquired evolution equation, first the linear stability analysis is performed and nonlinear surface-wave behavior is then investigated by a numerical computation using a Fourier-spectral method.

The following sections are composed of formulation, thin film limit, linear stability analysis, nonlinear film evolution and conclusions. In the section of formulation, the flow configuration and governing equations in both of liquid and vapor phases are explained. The section of thin film limit shows the asymptotic approaches to the governing equations to get a nonlinear evolution equation for the film height. From the transient, spatially uniform and basic state, linear stability analysis has been performed by introducing a small disturbance into the free surface in the section of linear stability analysis. The various nonlinear surface-wave evolutions are computed in the section of nonlinear film evolution, and in the final section the results are concluded.

FORMULATION

The flow is considered of an incompressible, viscous, thin liquid film draining down an inclined plane with gravity g. The plane is assumed to make an angle β with the horizontal, and the two-dimensional coordinate system is chosen such that the x axis is parallel to the plane and the y axis is perpendicular to it. Above the liquid film there is an air phase with a pressure p_a, where at a distance H from the plane is a charged plate parallel to the x axis. The electric field generated from the charged plate acts in the direction normal to the inclined plane. Let x=0 be at the center of the charged plate. The film thickness in the primary flow is defined as d and ξ=d/L, where L is the characteristic length scale parallel to the film (Fig. 1).

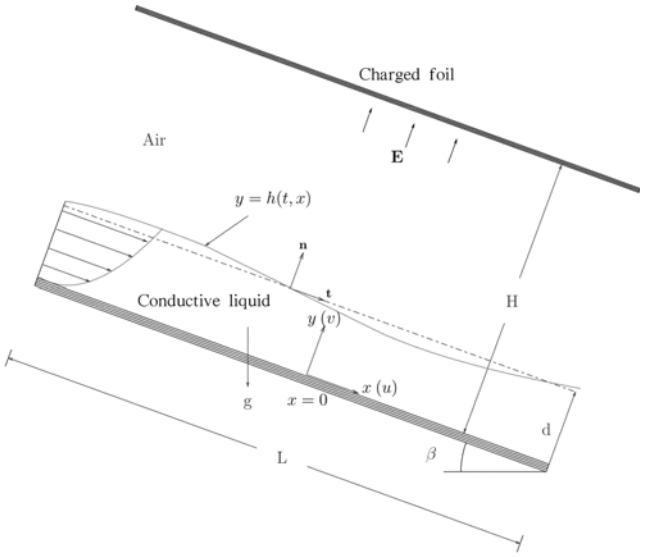

Fig. 1. The coordinate scheme for the plane flow at a high Reynolds number under an electrostatic field.

The electric field is satisfied by Laplace's equation,

$$\nabla^2\phi=0, \tag{1}$$

for the electric potential ϕ(x, y) in the fluid, ϕ^f, and for that in the air region, ϕ^v. To solve this equation the following boundary conditions are needed:

$$\phi(x, H)=FH\Phi(x), \text{ for } y=H, \ \phi=0, \text{ for } y=0, \tag{2}$$

and along the free surface y=h(x, t) the interfacial boundary conditions are

$$\phi^f(x, h, t)=\phi^v(x, h, t), \ \varepsilon_f\mathbf{n}\cdot\nabla\phi^f=\varepsilon_0\mathbf{n}\cdot\nabla\phi^v. \tag{3}$$

Here ε_f is the dielectric constant of the fluid, ε_0 is that of the air and **n** is the outward unit normal to the interface.

The independent and dependent variables used in the governing equations of liquid motion and the evolution equations are expressed in non-dimensional forms by letting d be the unit of length in the y direction, L the unit of length in the x direction, U_0, which will be chosen later, the unit of the x-direction velocity u, ξU_0 the unit of the y-direction velocity v, L/U_0 the unit of time t, ρU_0^2 the unit of pressure p where ρ is the fluid density, F the unit of electric field and FH the unit of electrostatic potential. The continuity equation is

$$u_x+v_y=0, \tag{4}$$

while the x and y components of the momentum equation are

$$\xi(u_t+uu_x+vu_y)=-\xi p_x+\frac{1}{\mathrm{Re}}(\xi^2u_{xx}+u_{yy})+\frac{\sin\beta}{\mathrm{Fr}^2} \tag{5}$$

and

$$\xi^2(v_t+uv_x+vv_y)=-p_y+\frac{\xi}{\mathrm{Re}}(\xi^2v_{xx}+v_{yy})-\frac{\cos\beta}{\mathrm{Fr}^2}. \tag{6}$$

Here u and v are the velocity components of x and y directions, respectively, and p is the pressure. The subscripts represent the partial derivatives. And we have introduced the Reynolds number

$$\mathrm{Re}=\frac{\rho U_0 d}{\mu}, \tag{7}$$

where μ is the fluid viscosity. The Froude number is defined as

$$\mathrm{Fr}=\frac{U_0}{\sqrt{gd}}. \tag{8}$$

We still need the boundary conditions to solve the Navier-Stokes equations. The no-slip boundary conditions along the solid wall of y=0 are

$$u=0, \ v=0. \tag{9}$$

On the interface of y=h(x, t), we have three more boundary conditions: the continuity of normal stress [3]

$$\xi^2\mathrm{We}\ h_{xx}[1+\xi^2h_x^2]^{-\frac{3}{2}}=p_a-p+\frac{2\xi}{\mathrm{Re}}[\xi^2h_x^2u_x-h_x(u_y+\xi^2v_x)+v_y]$$
$$[1+\xi^2h_x^2]^{-1}+\frac{2K}{\mathrm{Re}}\left(\frac{1}{\varepsilon_f}-1\right)[(E_n^v)^2+\varepsilon_f(E_t^v)^2], \tag{10}$$

the continuity of tangential stress

$$[1-\xi^2 h_x^2](u_y+\xi^2 v_x)+2\xi^2 h_x(v_y-u_x)=0, \tag{11}$$

and the kinematic condition

$$h_t+u\,h_x=v. \tag{12}$$

Here we have introduced the Weber number,

$$We=\frac{\sigma}{\rho U_0^2 d}, \tag{13}$$

where σ is the surface tension of fluid and d is the unperturbed uniform flow depth. The dimensionless electrostatic constant

$$K=\frac{\varepsilon_0 dF^2}{16\pi\mu U_0}. \tag{14}$$

The pressure in the air above the liquid film is set p_a, and the normal and tangential components of the electric field in the air are defined as $E_n^v=\mathbf{E}^v\cdot\mathbf{n}$ and $E_t^v=\mathbf{E}^v\cdot t$, respectively, where $\mathbf{t}$ is the unit tangent to the interface and the dimensionless electric field vector is

$$\mathbf{E}^v=\left(\zeta\frac{\partial\phi^v}{\partial x},H\frac{\partial\phi^v}{\partial y}\right). \tag{15}$$

Here ζ=H/L.

THIN FILM LIMIT

From now on we will consider the thin film limit, ξ<<1, of Eq. (1)-(12) and derive a nonlinear evolution equation for the height, h(x, t). For the applications under consideration a larger Reynolds number may be necessary. Hence here we treat the thin film limit with Re=O(1/ξ), i.e., ξRe=R=O(1). We will assume ξ^2We=W≃ O(1) to include the effect of surface tension in the leading order term. And we now consider the β small limit and define B=ξcotβ=O(1) and K=O(1). In this limit the inertial terms appear at lowest order, and it is necessary to use the von Kármán-Pohlhausen approximation to obtain an evolution equation. This has successfully been applied to other thin film problems in the absence of electric field (Rahman et al. [12] and Prokopiou et al. [13]). Here we have employed the second-order integral boundary-layer approximation first considered by Prokopiou et al. [13] where, however, they have not included all the second-order terms in both of y-momentum and normal-stress equations. In their model the y-momentum balance is assumed to be dominated only by hydrostatic forces. In our analysis we have included all of the second-order terms in the governing and boundary equations and will discuss these terms in detail later. The local x-component velocity is approximated by the self-similar profile

$$u=\frac{3Q}{h}\left\{\frac{y}{h}-\frac{1}{2}\left(\frac{y}{h}\right)^2\right\}, \tag{16}$$

where Q is the local flow rate defined by

$$Q=\int_0^h u\,dy. \tag{17}$$

With Eq. (16) the y-component velocity from Eq. (4) is obtained as

$$v=-y^2\left(\frac{3Q_x}{2h^2}-\frac{3h_xQ}{h^3}\right)+y^3\left(\frac{Q_x}{2h^3}-\frac{3h_xQ}{2h^4}\right). \tag{18}$$

And with the above results we can get the pressure from Eq. (6) using the normal stress boundary condition Eq. (10). The result up to O(ξ^2) is

$$\begin{aligned}p=p_a+&\frac{\cos\beta}{Fr^2}(h-y)-Wh_{xx}-\frac{2K}{R}(E_{0n}^v)^2\xi+\Big[\Big(\frac{3Qh_x}{2Rh^2}-\frac{3Qh_xh_t}{2h}\\&+\frac{5Q_th_x}{8}-\frac{33Q^2h_x^2}{40h^2}-\frac{3Q_x}{2Rh}+\frac{5Q_xh_t}{8}+\frac{3QQ_xh_x}{20h}+\frac{Q_x^2}{2}+\frac{5Qh_{xt}}{8}\\&-\frac{3Q_{xt}h}{8}+\frac{33Q^2h_{xx}}{40h}+\frac{3h_x^2h_{xx}}{2}W-\frac{QQ_{xx}}{2}\Big)-\Big(\frac{3Q_x}{Rh^2}-\frac{6Qh_x}{Rh^3}\Big)y\\&+\Big(\frac{3Q_x}{2Rh^3}-\frac{9Qh_x}{2Rh^4}\Big)y^2+\Big(\frac{3Qh_xh_t}{h^4}-\frac{Q_th_x}{h^3}-\frac{Q_xh_t}{h^3}-\frac{Qh_{xt}}{h^3}+\frac{Q_{xt}}{2h^2}\Big)y^3\\&+\Big(\frac{3Q_th_x}{8h^4}-\frac{3Qh_th_x}{2h^5}+\frac{9Q^2h_x^2}{4h^6}+\frac{3Q_xh_t}{8h^4}-\frac{9Q_x^2}{8h^4}+\frac{3Qh_{xt}}{8h^4}-\frac{Q_{xt}}{8h^3}\\&-\frac{9Q^2h_{xx}}{4h^5}+\frac{9QQ_{xx}}{8h^4}\Big)y^4+\Big(-\frac{9Q^2h_x^2}{5h^7}-\frac{3QQ_xh_x}{20h^6}+\frac{3Q_x^2}{4h^5}+\frac{9Q^2h_{xx}}{5h^6}\\&-\frac{3QQ_{xx}}{4h^5}\Big)y^5+\Big(\frac{3Q^2h_x^2}{8h^8}-\frac{Q_x^2}{8h^6}-\frac{3Q^2h_{xx}}{8h^7}+\frac{QQ_{xx}}{8h^6}\Big)y^6\Big]\xi^2.\end{aligned} \tag{19}$$

We will set the electric potential along y=H to a constant value of one and take the characteristic length scale in the y direction in the air region as d. Hence, the leading-order electric field can be transformed from the electrostatic potential at leading order in ξ, i.e., $E_{0n}^v=H(\partial\phi_0^v/\partial y)$, where ϕ_0^v is derived from the Eq. (1) with the boundary conditions (2) and (3):

$$\phi_0^v=\left\{1+(y-H)\left[h(x,t)\left(\frac{1}{\varepsilon_f}-1\right)+H\right]^{-1}\right\},\quad \text{for } h(x,t)<y<H. \tag{20}$$

Finally, after integrating Eq. (5) in y from 0 to h with the help of Eq. (16), Eq. (18) and Eq. (19) at the specified boundary conditions, we have obtained a coupled set of nonlinear hyperbolic system of equations accurate to O(ξ^3) for the height h and flow rate Q. The results are as follows:

$$h_t=-Q_x \tag{21}$$

and

$$\begin{aligned}&Q_t+\frac{\partial}{\partial x}\left(\frac{6Q^2}{5h}\right)+\frac{3h}{R}(Bh_x-1)+\frac{3Q}{Rh^2}-Whh_{xxx}\\&-\frac{2h}{R}K\left(1-\frac{1}{\varepsilon_f}\right)\frac{\partial}{\partial x}(E_{0n}^v)^2\xi+\Big[-\frac{9Q_{xx}}{2R}+\frac{6Qh_{xx}}{Rh}\\&-\frac{6Qh_x^2}{Rh^2}+\frac{6h_xQ_x}{Rh}+\frac{783}{350}\frac{Qh_x^2}{h}\Big(Q_x-\frac{Qh_x}{2h}\Big)-\frac{443}{700}Q_x^2h_x\\&+\frac{27}{50}(Q^2h_x-2QQ_xh)\Big(\frac{h_x^2}{h^2}+\frac{h_{xx}}{h}\Big)+\frac{108}{175}\frac{Q^2h_xh_{xx}}{h}\\&+\frac{613}{1400}QQ_xh_{xx}-\frac{489}{350}QQ_{xx}h_x+\frac{1417}{1400}Q_xQ_{xx}h+\frac{51}{175}Q^2h_{xxx}\\&-\frac{241}{1400}QQ_{xxx}h+3Whh_xh_{xx}^2+\frac{3}{2}Whh_x^2h_{xxx}\Big]\xi^2=0.\end{aligned} \tag{22}$$

Here we have used the characteristic velocity U_0 as the average entrance velocity of the primary flow, i.e., $U_0=\rho g d^2\sin\beta/3\mu$, and from the definitions of the dimensionless constants it has to be noted

$$\frac{R\cos\beta}{3Fr^2B}=1. \tag{23}$$

During the derivation of Eq. (22) we have used spatial derivative

forms of h and Q instead of Q_t appearing in the integration procedure of the second-order terms, by assuming Q_t is only balanced with inertial force, that is, $Q_t=-(6/5Q^2/h)_x$. This is pertinent because the inertial force is dominating over other forces in a large Reynolds number flow. Comparing the result from Prokopiou et al. [13] with Eq. (22) we have many additional terms attributed to including the inertial forces, i.e., $v_t+uv_x+vv_y$ in the y-momentum Eq. (6) which were not considered by Prokopiou et al. In addition, note we have the viscous dissipation term of 9/2 Q_{xx}/R while Prokopiou et al. had the value of 5 Q_{xx}/R because they did not include v_{yy} in the y-momentum equation. They simply assumed the y-direction pressure gradient was only balanced by hydrostatic force. However, in our model we have all of the second-order terms considered. In Eq. (22) the viscous dissipation terms contain second derivatives of Q and h with respect to x.

LINEAR STABILITY ANALYSIS

As the liquid layer is running down an inclined plane it can be easily disturbed and nearly periodic surface waves are observed along the downstream. During the formation of these waves it is interesting to study the evolution of the waves initially excited with a small amplitude as time marches. The growth rate can be predicted by the linear stability analysis while the waves propagate downstream. In case of a non-electrified flowing layer the surface tension and the hydrostatic pressure act as stable factors, whereas the mean shear flow makes the film unstable.

Before we continue the linear stability analysis based on the two-dimensional film flow, we have to answer the validity question about the two-dimensional analysis which may be raised in the linear stability analysis. According to Squire's theorem, in the plane Poiseuille flow three-dimensional disturbance is less unstable than two-dimensional one and there exists a transformation between the two cases [14]. However many flow regimes have been proven not to be subjected to Squires theorem, especially where the gas-liquid interface is involved. Nevertheless, it is also worth noticing that Blyth [11] has concluded that, in his stability analysis on the contaminated film flow under an electric field, it was sufficient to consider two-dimensional analysis for an accurate estimation of the critical Reynolds number based on his extended form of Squire's theorem. Since Blyth's configuration of the flow system is exactly the same as ours except for the Marangoni effect due to the concentration of insoluble surfactants, we will just here cite his validity remarks to confine our stability analysis to two-dimensional perturbations.

To perform the linear stability analysis a basic state has to be sought. It can be seen from Eq. (21) and Eq. (22) h=1 and Q=1. Until now we have employed the small parameter ξ to determine each physical term's significance to the flow, but now we will consider the scaling factor in both x- and y-directions is d in the linear stability analysis since the linear stability has its own assumption of the long wave approximation. Thus we can take ξ=1 in the hyperbolic equations. Letting η represent the perturbation of h from the uniform height, i.e., h=1+η, we can derive the linearized disturbance equation from Eq. (21) and Eq. (22):

$$\frac{3}{R}\eta_t+\eta_{tt}+\frac{9}{R}\eta_x+\frac{12}{5}\eta_{xt}+\frac{6}{5}\eta_{xx}-\frac{3B}{R}\eta_{xx}$$
$$-\frac{4}{R}K\left(1-\frac{1}{\varepsilon_f}\right)\frac{H^2(1/\varepsilon_f-1)}{\{H+(1/\varepsilon_f-1)\}^3}\eta_{xx}+W\eta_{xxxx}$$
$$-\left(\frac{9}{2R}\eta_{xxt}+\frac{6}{R}\eta_{xxx}+\frac{11}{40}\eta_{xxtt}+\frac{233}{280}\eta_{xxxt}+\frac{87}{140}\eta_{xxxx}\right)=0. \quad (24)$$

Looking for a time harmonic solution proportional to $\eta=e^{[i(\alpha x-ct)]}$, where α is the real wavenumber and $c=c_r+ic_i$ is the complex wave frequency, we find from Eq. (24) the dispersion relation

$$c^2\left(1+\frac{11\alpha^2}{40}\right)-c\left\{\frac{12\alpha}{5}+\frac{233\alpha^3}{280}-i\left(\frac{3}{R}+\frac{9\alpha^2}{2R}\right)\right\}$$
$$+\frac{6\alpha^2}{5}-\frac{3B\alpha^2}{R}-\frac{4}{R}K\left(1-\frac{1}{\varepsilon_f}\right)\frac{H^2(1/\varepsilon_f-1)}{\{H+(1/\varepsilon_f-1)\}^3}\alpha^2$$
$$-W\alpha^4+\frac{87}{140}\alpha^4-i\left(\frac{9\alpha}{R}+\frac{6\alpha^3}{R}\right)=0. \quad (25)$$

After expanding c with α we obtained the asymptotic solution of real and imaginary part of c up to order of α^2. The solution of c is

$$c=3\alpha-\frac{1}{3}i\alpha^2R\left\{-3+\frac{3B}{R}+\frac{4}{R}K\left(1-\frac{1}{\varepsilon_f}\right)\frac{H^2(1/\varepsilon_f-1)}{\{H+(1/\varepsilon_f-1)\}^3}+W\alpha^2\right\}, \quad (26)$$

where we consider $W=O(\alpha^{-2})$ again.

The sign of c_i determines the linear stability of the flow. If $c_i>0$, the flow is unstable and if $c_i<0$, the flow is stable. When $c_i=0$, we obtain the critical Reynolds number as

$$R_c=\left[B+\frac{4}{3}K\left(1-\frac{1}{\varepsilon_f}\right)\frac{H^2(1/\varepsilon_f-1)}{\{H+(1/\varepsilon_f-1)\}^3}\right]\left(1-\frac{1}{3}W\alpha^2\right)^{-1}. \quad (27)$$

The critical Reynolds number has a little different value from the small Reynolds-number theory of Kim [4] where the critical Reynolds number Re_c is obtained as

$$Re_c=\frac{5}{6}\cot\beta+\frac{10}{9}W\alpha^2+\frac{5}{9}K\left(1-\frac{1}{\varepsilon_f}\right)\frac{H^2(1/\varepsilon_f-1)}{\{H+(1/\varepsilon_f-1)\}^3}. \quad (28)$$

This is not so unexpected because of the difference in the order of Reynolds number and of the approximation Eq. (16) used for the velocity profile.

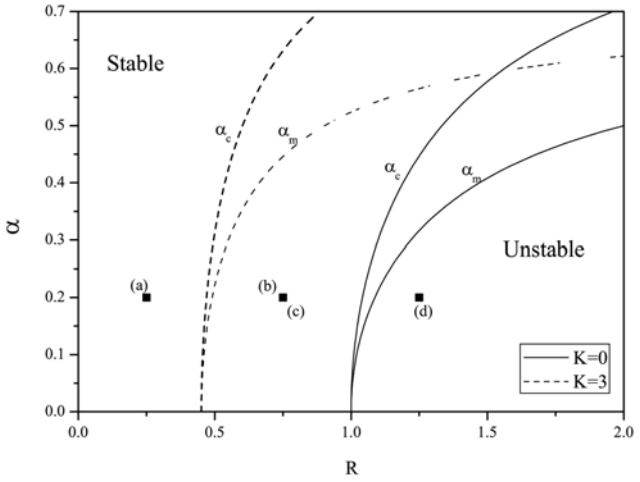

Fig. 2. Neutral stability curves in (R, α) domain for B=1, H=10 and W=3.

In addition, the maximum growth rate showing the greatest amplitude-growing rate of surface-wave disturbance is also obtained in (α, R) domain from $d(c_i)/d\alpha=0$. The result is

$$R=\left[B+\frac{4}{3}K\left(1-\frac{1}{\varepsilon_f}\right)\frac{H^2(1/\varepsilon_f-1)}{\{H+(1/\varepsilon_f-1)\}^3}\right]\left(1-\frac{2}{3}W\alpha^2\right)^{-1}. \quad (29)$$

The cutoff wavenumber α_c from Eq. (27) and maximum-growth-rate wavenumber α_m from Eq. (29) corresponding to R are plotted in Fig. 2 for both K=3 (dashed line) and K=0 (solid line), H=10, B=1, and W=3. Here the liquid is considered a perfect conductor ($\varepsilon_f=\infty$). Several Reynolds numbers such as R=0.25(a), 0.75((b) and (c)) and 1.25(d) throughout the stable and unstable regions are selected at a fixed wavenumber α=0.2 to confirm whether the expectation from this linear stability analysis is true or not. The effect of an electrostatic field is shown to increase both Reynolds numbers showing the critical and maximum growth rates at a given wavenumber.

NONLINEAR FILM EVOLUTION

The linear stability analysis is only true while the perturbed surface maintains a long wave length compared with its amplitude. However, as the linear wave evolves into the downstream it is affected by the nonlinear effects and the linear analysis is not valid any more. Thus to investigate the nonlinear effects on the surface wave, the derived nonlinear evolution equations of (21) and (22) have to be solved numerically. In a small Reynolds number flow under the influence of an electrostatic field Kim [4] solved a nonlinear evolution equation depicting the film variations numerically by a Fourier-spectral method. The initially computed surface-wave instability was coincided with the result from the linear stability analysis. Kim [4] also showed the nonlinear modal interactions between the harmonics with higher frequencies.

The evolution equations of (21) and (22) consist of a nonlinear hyperbolic system of partial differential equations and one needs two initial values in the laterally unbounded domain. As an initial wave shape, a sinusoidal disturbance of small amplitude has been chosen to confirm the validity of the surface-wave developments as predicted by linear theory:

$$h(0, x)=1-0.1\cos(\alpha x) \quad (30)$$

and the initial local flow rate Q has taken with the same form as h. It makes the computational domain spatially periodic. To solve the

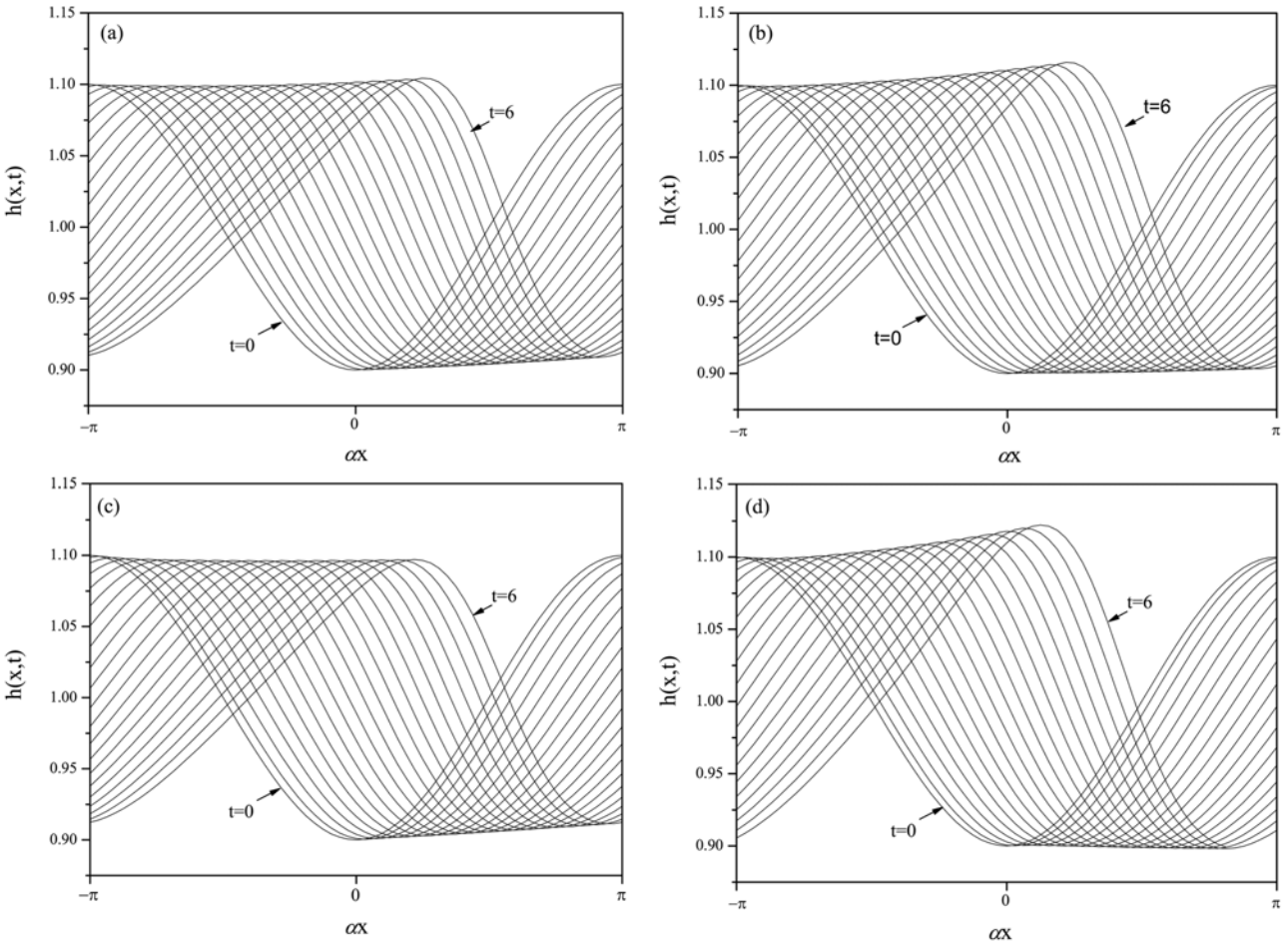

Fig. 3. Surface-wave behavior predicted from the linear stability analysis for α=0.2, B=1, H=10 and W=3. Free surfaces are plotted at every t=0.3.
(a) free-surface configurations at R=0.25 and K=3; (b) free-surface configurations at R=0.75 and K=3; (c) free-surface configurations at R=0.75 and K=0; (d) free-surface configurations at R=1.25 and K=0

evolution equations numerically, a Fourierspectral method is useful, i.e., the layer thickness h(t, x) and the flow rate Q(t, x) are calculated by the finite Fourier series, respectively, as

$$h(t,x)=\sum_{n=-N}^{n=N} a_n(t)\exp(i\alpha nx)+\text{complex conjugate} \quad (31)$$

and

$$Q(t,x)=\sum_{n=-N}^{n=N} b_n(t)\exp(i\alpha nx)+\text{complex conjugate} \quad (32)$$

with $N\geq 2^5$. The computational domain is set to $-\pi/\alpha\leq x\leq\pi/\alpha$. The solution for the time is calculated by a fourth-order modified Hamming's predictor-corrector method with the maximum tolerance of 10^{-12} using the fourth-order Runge-Kutta method for some initial predicting values. First, in Fig. 3 the evolutions of the interface have been computed with or without the effect of an electrostatic field in order to check the stability behavior as predicted in the linear theory. We have α=0.2 fixed throughout this computation. Under the influence of an electrostatic field R=0.25(a) and R=0.75(b) in Fig. 2 are adopted to represent stability and instability, respectively. In case of no electrostatic field we have selected R=0.75(c) and R=1.25(d) in Fig. 2 to demonstrate the stable and unstable surface wave behaviors, respectively. In the electrified case, as we can see in Fig. 3(a) with a stable R=0.25, the initially disturbed surface wave decays slightly as time lapses while the disturbance at an unstable R=0.75 grows linearly as seen in Fig. 3(b). In the absence of an electrostatic field Fig. 3(c) and 3(d) show also well the predictions from the analysis of linear stability, that is, at the stable R=0.75 the amplitude of surface wave becomes down while contrary to this the wave at R=1.25 lying in the unstable region becomes unstable. Here it is noted even at the same Reynolds number R=0.75 the instability has been changed from an unstable mode (Fig. 3(b)) to a stable one (Fig. 3(c)).

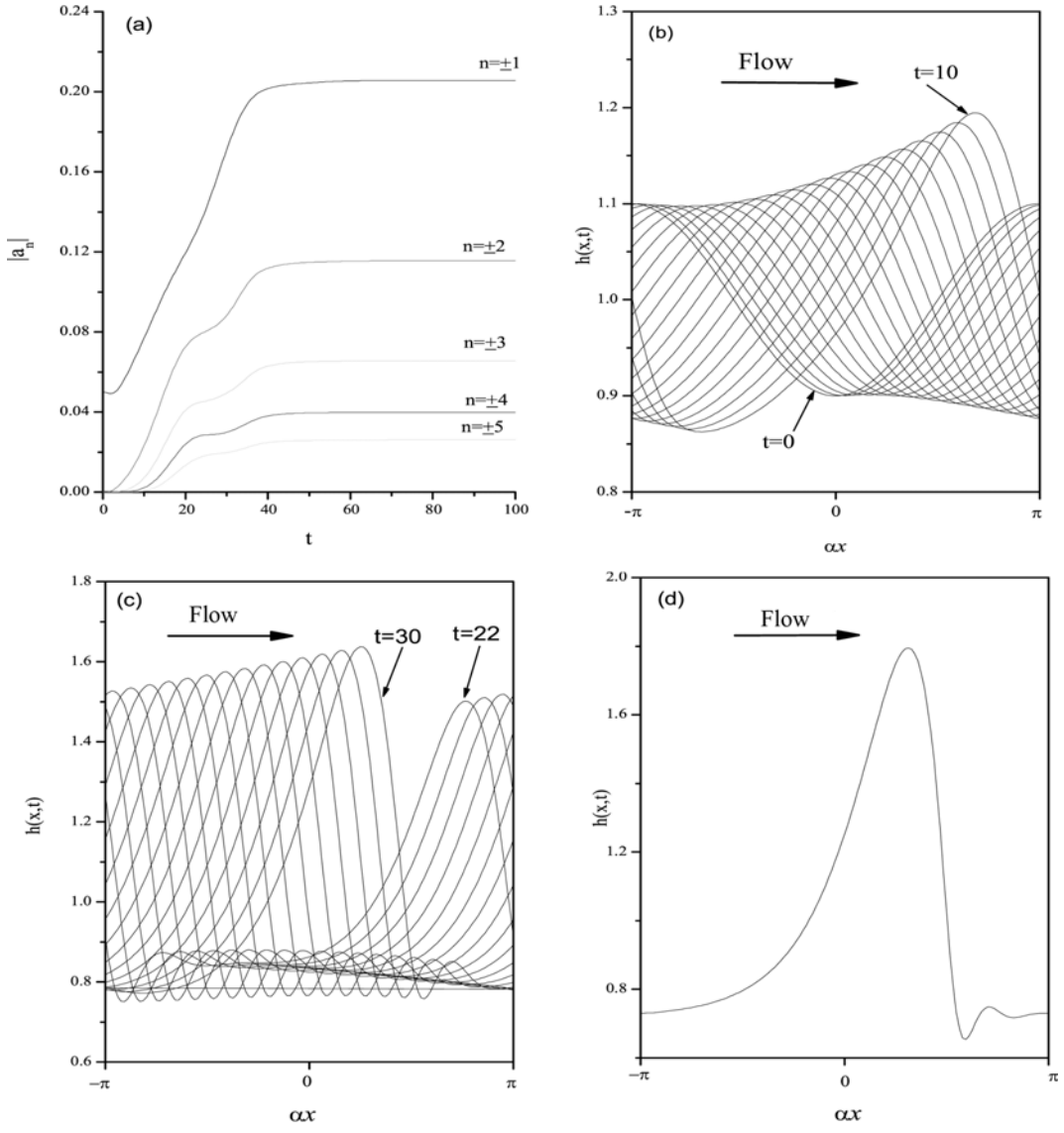

Fig. 4. Surface-wave behavior for α=0.2, Q_0=1, R=5, B=1, K=3, H=10 and W=3. Free surfaces are plotted at every t=0.5 for (b) and (c). (a) evolution of Fourier-spectral coefficients; (b) free-surface configurations for 0≤t≤10; (c) free-surface configurations for 22≤t≤30; (d) a pulse-like solitary wave at t=90

Hence, we can understand the electrostatic field makes the film flow at a high Reynolds number more unstable at the same Reynolds number.

Next, to see the nonlinear dynamics of the film evolution we have traced the surfacewave deformations according to various electrostatic field constants by changing an initial flow rate Q_0. If we take $Q_0>1$ it can be expected the film flow has the same effect of an injection from the inlet point. Hence, the augmented initial flow rate will act as an unstable factor to the film flow as well as an applied electric field. Here during the exemplary calculations we have fixed α=0.2, R=5, B=1, H=10 and W=3. In Fig. 4 we have computed the evolution of Fourier-spectral coefficients of the surface waves up to n=±5 and the free-surface configurations with Q_0=1 and K=3. As we can see in Fig. 4(a) an initially disturbed wave with $|a_{\pm1}|$=0.05 and $|a_{\pm n}|$=0 (n>1) are getting excited and the lower harmonics are stirred and perturbed as time marches. The initial sinusoidal shape is distorted and amplified through the nonlinear modal interactions as in Fig. 4(b). Fig. 4(c) shows the wave front becomes steepened while the rear is stretching as time goes on. The surface waves are plotted at every t=0.5. As letting the film flow have enough time, the surface wave is not changed anymore and the shape looks like a solitary wave as in Fig. 4(d). Beyond a transition region from the initial inlet of the flow we can observe the disturbed sinusoidal waves evolve downstream into distinct pulse-like solitary waves over a comparatively long distance. Unlike the sinusoidal waves, the solitary wave has a wide band of Fourier harmonics whose phases are locked like in Fig. 4(a). Kim [5] addressed in details the characteristics of pulse-like solitary waves developing gradually under an electrostatic field in a small Reynolds number limit. In Fig. 5 we have an increased initial local flow rate Q_0=10 while keeping the other parameters to have the same ones as in Fig. 4. Fig. 5(a) describes the evolution of Fourier-spectral coefficients. Here we see the phases of Fourier harmonics are fixed in an earlier stage by comparing with Fig. 4(a), which means a pulselike solitary wave is brought into existence in advance as in Fig. 5(b). The greater inlet flow rate makes the surface wave more unstable because the surface wave residing on the upstream flow is pushing the surface ahead and inducing a buckling phenomenon. With a greater value of Q_0=15 we can observe a surface-wave breaking in Fig. 6. In Fig. 6(b) the amplitude of the disturbance grows super-exponentially due to the higher Fourier-spectral coefficients excited in the initial stage seen in Fig. 6(a). As the film height gets thicker, the local phase speed of the

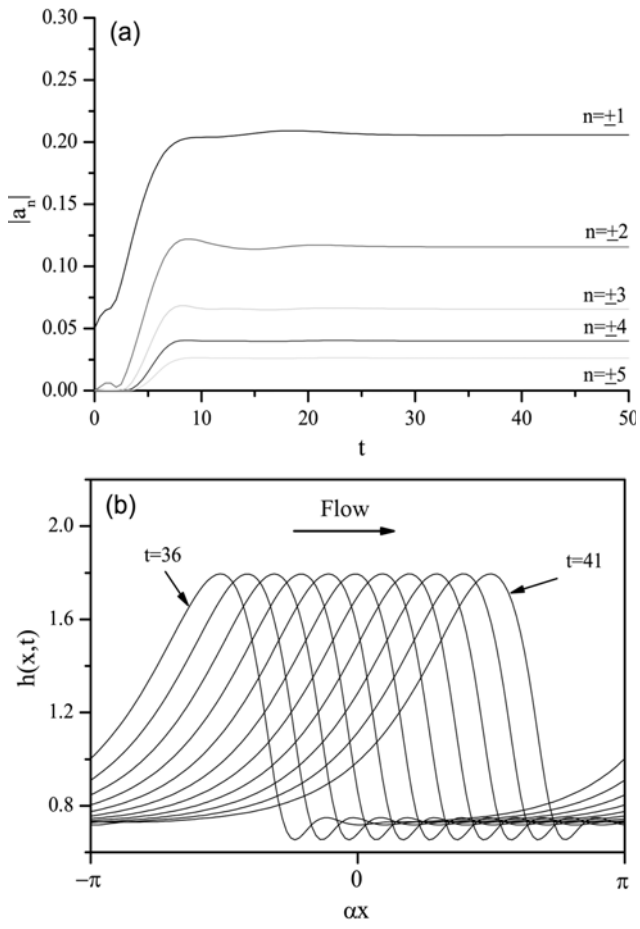

Fig. 5. Surface-wave behavior for α=0.2, Q_0=10, R=5, B=1, K=3, H=10 and W=3. Free surfaces are plotted at every t=0.5 for (b).
(a) evolution of Fourier-spectral coefficients; (b) free-surface configurations for 36≤t≤41

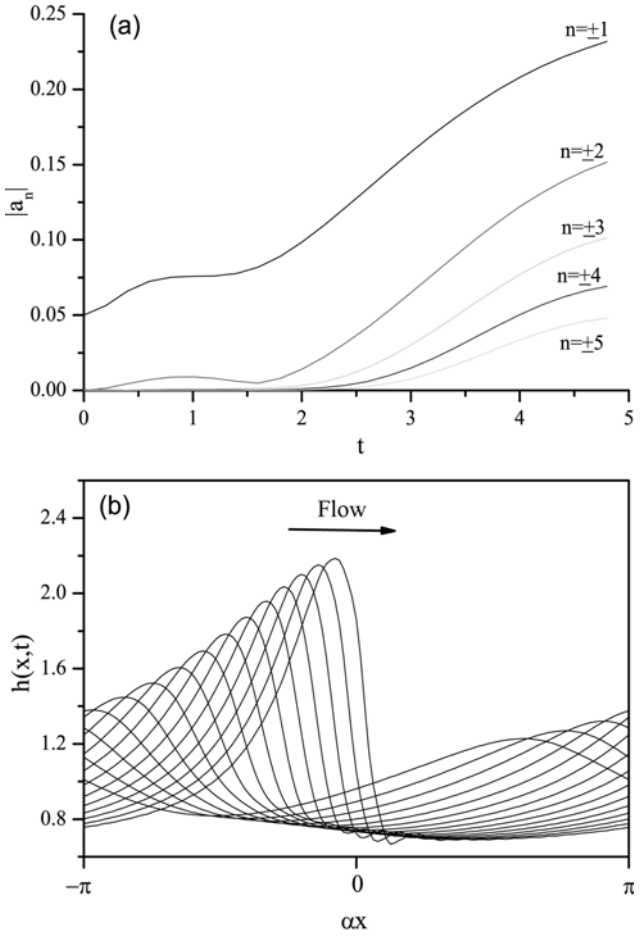

Fig. 6. Surface-wave behavior for α=0.2, Q_0=15, R=5, B=1, K=3, H=10 and W=3. Free surfaces are plotted at every t=0.2 for (b).
(a) evolution of Fourier-spectral coefficients; (b) free-surface configurations for 2.0≤t≤4.8

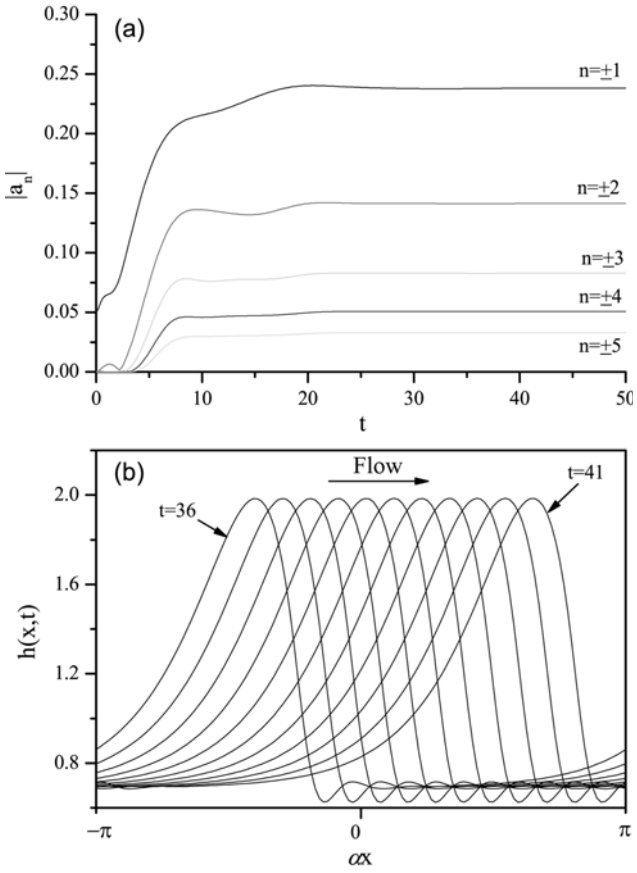

Fig. 7. Surface-wave behavior for α=0.2, Q_0=10, R=5, B=1, K=5, H=10 and W=3. Free surfaces are plotted at every t=0.5 for (b). (a) evolution of Fourier-spectral coefficients; (b) free-surface configurations for 36≤t≤41

surface wave is accelerating. Hence, the traveling speed of the crest is greater than that of the trough as shown in Fig. 6(b) where the wave front is getting steeper and steeper and results in a wave breaking. In addition, to see the effect of an electrostatic field on the surface-wave evolution we have applied a larger value of K, i.e., K=5 comparing with the case of Fig. 5 (K=3) while the other parameters are retained in the same. As in Fig. 7(a) the growing rates and magnitudes of Fourier-spectral coefficients are bigger than those in Fig. 5(a). Hence, by comparison of Fig. 5(b) (wave speed=3.19068 and crest height=1.795) with Fig. 7(b) (wave speed=3.33794 and crest height=1.984) we can see the greater electrostatic field has made the wave height get steeper and thicker which accelerated the speed of traveling waves. From this calculation of the nonlinear hydrodynamics the applied electrostatic field is also confirmed to make the flow more unstable as in the analysis of linear stability.

The nonlinear free-surface evolution has been calculated with various initial flow rates under two different electric fields and the growth rates are monitored by the Fourier-spectral coefficients. We have observed greater flow rates and electrostatic fields make the film flow more unstable. In addition, one thing to note is that the nonlinear hyperbolic system of equations derived by the second-order boundary-layer theory includes the dissipation terms containing second derivatives of Q and h with respect to x which make it possible to have solitary waves easily. Without the dissipation terms this high Reynolds number flow did not allow periodic and solitary waveforms [13]. These calculations are not necessarily physically realistic and just show the nondimensional parametric results.

CONCLUSIONS

To answer the questions on the stabilities of thin liquid flows at high Reynolds numbers interacting with an overlying uniform electrostatic field, we have derived evolution equations describing the free-surface behavior by using the von Kármán-Pohlhausen approximation. The nonlinear hyperbolic system of equations is developed by a second-order integral boundary-layer theory for long waves at large Re of $O(\xi^{-1})$ to include the dissipation terms which allow periodic and solitary waves. By applying a small perturbation having a timeharmonic wave mode to a basic state which is a uniform flat layer, a linear stability analysis has been performed. We obtained a little different critical Reynolds number from the small Reynolds number approximation. From this analysis we have known the applied electrostatic field acts as an instability. The instability can be inferred from the steady-state solutions of Eq. (21) and Eq. (22). To get an analytical approach we will take those equations up to the first order of ξ. From Eq. (21) we get Q=1 and then the steady-state solution is determined from Eq. (22),

$$h_x\left[\frac{3B}{R}h^3-\frac{6}{5}-\frac{4\xi K}{R}\frac{H^2}{\{H+h(1/\varepsilon_f-1)\}^3}h^3\right]=\frac{3}{R}(h^3-1)+Wh^3h_{xxx}. \quad (33)$$

This steady-state solution will have a point where there is an infinite slope making a shock, when the coefficient of the first derivative term is zero. Therefore, we can find a critical height, h_c, as a function of the parameters. Solving for h_c involves solving a sixth-order polynomial in h. Hence suppose we only consider the limit where H≫h. The result with $\varepsilon_f=\infty$ is

$$h_c=\left[\frac{6}{5}\frac{R}{3B-4\xi K/H}\right]^{1/3}. \quad (34)$$

We can see the effect of the electric field is to raise h_c, which means the flow becomes more unstable.

To overcome the limit of the linear stability analysis, which is only valid at the longwave approximation, nonlinear stability has been also performed with the aid of numerical computation. The computational domain is taken as a spatially periodic and the evolution equations are numerically solved by a Fourier-spectral method. At the inception of the computation the nonlinear outputs are well matched to the results from the linear stability analysis. The nonlinear free-surface evolution has been computed with various initial flow rates to confirm the nonlinear hydrodynamics. The greater the flow rates that are imposed on the film flow the more unstable surface waves are observed. It is also demonstrated that the applied electrostatic strength plays the role of an instability. Note that without a wave breaking, the large Reynolds number flow always create a pulse-like solitary waveform which is not easily developed in a small Reynolds-number flow [5].

ACKNOWLEDGMENT

This study was performed by support from the University of Seoul

in 2008, and the authors gratefully acknowledge it.

NOMENCLATURE

B : $\cot\beta$
d : characteristic film thickness
E : dimensionless electric field vector
F : electrostatic potential
Fr : Froude number
g : gravity
H : dimensionless distance from plane to charged plate
h : dimensionless local film thickness
K : dimensionless electric force constant
L : characteristic length scale parallel to plane
n : unit normal vector
p : dimensionless pressure
p_a : dimensionless air pressure
Q : dimensionless local flow rate
R : ξRe
Re : Reynolds number
t : unit tangent vector
t : dimensionless time
U_0 : characteristic velocity
u : dimensionless velocity in x direction
v : dimensionless velocity in y direction
W : ξ^2We
We : Weber number
x : dimensionless distance coordinate parallel to plane
y : dimensionless distance coordinate perpendicular to plane

Greek Letters

α : wave number
β : inclination angle of plane with the horizontal
ε : $\varepsilon_f/\varepsilon_0$
ε_0 : dielectric constant of air
ε_f : dielectric constant of liquid
ζ : H/L
η : perturbation of h
μ : viscosity of liquid
ξ : d/L
ρ : mass density of liquid
σ : surface tension of liquid
ϕ : electric potential

Superscripts

f : fluid
v : air

Subscripts

c : critical value
t : partial derivative with t
x : partial derivative with x

REFERENCES

1. T. B. Benjamin, *J. Fluid Mech*., **2**, 554 (1957).
2. C. -S. Yih, *Phys. Fluids*, **5**, 321 (1963).
3. H. Kim, S. G. Bankoff and M. J. Miksis, *Phys. Fluids A*, **4**, 2117 (1992).
4. H. Kim, *Korean J. Chem. Eng*., **14**, 41 (1997).
5. H. Kim, *Korean J. Chem. Eng*., **20**, 803 (2003).
6. K. S. Kim and H. Kim, *Korean J. Chem. Eng*., **25**, 25 (2007).
7. E. M. Griffing, S. G. Bankoff, M. J. Miksis and R. A. Schluter, *ASME I: J. Fluids Engng*, **128**, 276 (2006).
8. E. Schäffer, T. Thurn-Albrecht, T. P. Russell and U. Steiner, *Nature*, **403**, 874 (2000).
9. E. Schäffer, T. Thurn-Albrecht, T. P. Russell and U. Steiner, *Europhys. Lett*., **53**, 518 (2001).
10. Z. Lin, T. Kerle, E. Schäffer, U. Steiner and T. P. Russell, *Macromolecules*, **35**, 3971 (2002).
11. M. G. Blyth, *J. Fluid Mech*., **595**, 221 (2008).
12. M. M. Rahman, A. Faghri, W. L. Hankey and T. D. Swanson, *Proc. Natl. Heat Transfer. Conf*., **110**, 161 (1989).
13. Th. Prokopiou, M. Cheng and H.-C. Chang, *J. Fluid Mech*., **222**, 665 (1991).
14. S. G. Yiantsios and B. R. Higgins, *Phys. Fluids*, **31**, 11 (1988).